Ferroelectrics, 370:18–28, 2008

ISSN: 0015-0193 print / 1563-5112 online
DOI: 10.1080/00150190802380268

Taylor & Francis
Taylor & Francis Group

Scattering and Depolarization in a Polymer Dispersed Liquid Crystal Cell

JUAN M. BUENO,[1] MARIS OZOLINSH,[2,*]
AND GATIS IKAUNIEKS[2]

[1]Laboratorio de Óptica (CiOyN), Universidad de Murcia, Campus de Espinardo 30100, Murcia, Spain
[2]Institute of Solid State Physics, University of Latvia, LV-1063 Riga, Latvia

An imaging polarimeter in transmission has been used to explore the effects of scatter and depolarization induced by a polymer dispersed liquid crystal cell. The experiment was carried out for three visible wavelengths. Both a directional and a scattered component can be distinguished in the light transmitted by this material. Whereas the directional component increased with voltage, the scattered portion decreased. This was a common behaviour for all three wavelengths. The polarimetric analysis revealed that the degree of polarization was also affected by changes in the voltage applied to the cell. Depolarization effects in the scattered component were usually high and decreased with voltage. However those associated with the directional part were low for high voltages and increased when reducing the voltage.

Keywords Polarimetry; Stokes vector; scattering; depolarization

1. Introduction

There is current interest in understanding the effects of scattering media on polarization and light propagation. Polarization-difference imaging and polarization gating methods have been demonstrated to be efficient in improving images through turbid media [1–4]. Mueller matrix polarimetry has successfully been used to extract the properties of the back-reflected light from highly scattered media for different particles sizes [5–8]. Moreover, it has been recently reported that scatter and depolarization are closely related to each other [9]. This offers a tool to investigate the effect of scatter by computing the degree of polarization (DOP) of the light emerging from an optical system. More recently the Stokes vector has been used to determine the scattering coefficient from polarized images of turbid media [10].

Since the image given by an optical system will be affected by the amount of scattering present, the characterization of this scattering is very important in order to determine the optical performance of the system. The human eye is an example of interest where effects of scatter occur and these change with aging and refractive surgery, among other factors [11, 12].

Received in final form September 3, 2007.
*Corresponding author. E-mail: ozoma@latnet.lv

On the other hand, polymer dispersed liquid crystal (PDLC) cells [13] are devices that can introduce different levels of scatter when changing the voltage. These have recently been used in vision research to simulate different stages of eye cataract [14].

In this work we present the results of experiments concerning the determination of optical properties of a PDLC cell in terms of scattering and depolarization. For this aim a multispectral imaging polarimeter has been developed.

2. Methods

2.1. Experimental Setup

The multispectral imaging polarimeter in transmission mode developed to characterize the PDLC cell is sketched in Fig. 1. The light source is a diode-pumped all-solid-state laser emitting at three different visible wavelengths (473, 532 and 635 nm). Along this work these wavelengths will be referred as blue, green and red respectively. The collimated laser beam passes through a fixed horizontal polarizer (P1) acting as generator unit. After passing through the sample under study (PDLC cell), the light enters the analyzer unit (AU) and reaches a semitransparent white screen (SC). AU is composed of a rotating retarder (RR) and a vertical polarizer (P2). A photographic objective (OB) makes SC conjugate with a CCD camera. The elements of AU can be removed independently from the system when necessary. If required the axis of P2 can also be oriented at any angle. The inset in Fig. 1 represents an alternative recording unit to measure only the directional component of the transmitted light (see Results section). This is composed of a 2-mm artificial aperture (AP), a positive lens (L, 50-mm focal length) and a photodetector (PHD).

PDLC cells consist of two glass plates with transparent electrodes forming a gap ($\sim$10 microns in thickness) of a composite polymer (PN393 *MerckKgaA*) with dispersed liquid crystal (BL035 *MerckKgaA*) droplets of micrometer size (references [13, 14] provide further information). The refractive index for the polymer was 1.473 (for $\lambda = 589$ nm). For the birefringent liquid crystal $n_o = 1.528$ and n_e is the same as for the polymer. These devices generate different levels of scattering when changing the applied AC voltage. If the applied voltage is null, liquid crystal droplets are randomly oriented and the difference between refractive indices of the polymer and liquid crystal causes light scattering. When applying

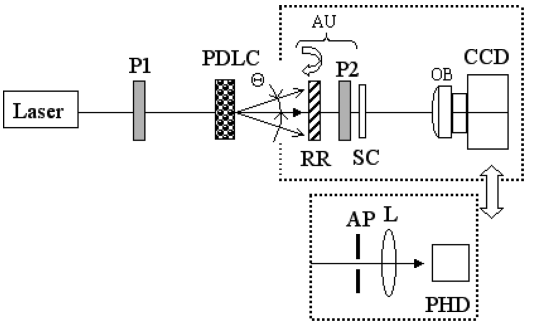

Figure 1. Schematic diagram of the imaging polarimeter. P1 and P2, linear polarizers; RR, rotating retarder; SC, white semitransparent screen; OB, objective. The inset represents an alternative recording stage composed of an aperture (AP), a positive lens (L) and a photodetector (PHD) (further information is included in the text).

an electric field, this aligns the liquid crystal droplets, the difference between the refractive indices diminishes and, consequently, PDLC transparency increases.

2.2. Experimental Procedure

In the first part of the experiment we analyzed the spatially resolved (or angular) dependence of the light transmitted through the PDLC as a function of the voltage and the wavelength. For these measurements the AU (RR plus P2) was removed from the experimental setup and we used both the CCD and the PHD (see Results for more information) for data registration.

In the second part, polarimetric measurements were carried out. We first started by testing the effect of the amount of scatter introduced by the PDLC on the Malus law. For this aim P2 was included in the light pathway. P2's transmission axis was rotated in increments of 10 degrees and images (when using the CCD) or intensities (when using the PHD) were recorded. This was repeated for blue, green and red light beams (see also below for further details).

Finally, P2's axis was set along the vertical direction and RR was introduced in the system to complete the AU. With this configuration the depolarization effects introduced by the PDLC cell were measured as explained in the following. Series of 4 images of the PDLC cell for each voltage and wavelength were recorded. Each image corresponded to an independent orientation of the fast axis of RR (−45, 0, 30 and 60 degrees) (see reference [9] for details). For each set of images the pixel-by-pixel Stokes vector (S_{OUT}) associated with the polarization state of light emerging from the PDLC cell was reconstructed using this equation:

$$S_{OUT} = \begin{pmatrix} S_0 \\ S_1 \\ S_2 \\ S_3 \end{pmatrix} = (M_{PSA})^{-1} \begin{pmatrix} I_1 \\ I_2 \\ I_3 \\ I_4 \end{pmatrix}, \tag{1}$$

where I_j (j = 1, 2, 3, 4) are the pixel values of the registered images and M_{PSA} is an auxiliary 4×4 matrix with each row being the first row of every Mueller matrix corresponding to an independent polarization state in the AU:

$$M_{PSA} = \frac{1}{2} \cdot \begin{pmatrix} 1 & -c & 0 & -s \\ 1 & -1 & 0 & 0 \\ 1 - \left(\frac{1}{4} + \frac{3}{4}c\right) & \frac{\sqrt{3}}{4}(c-1) & \frac{\sqrt{3}}{2}s \\ 1 - \left(\frac{1}{4} + \frac{3}{4}c\right) & -\frac{\sqrt{3}}{4}(c-1) & \frac{\sqrt{3}}{2}s \end{pmatrix}, \tag{2}$$

with c = cos$\delta(\lambda)$, s = sin$\delta(\lambda)$, and $\delta(\lambda)$ the retardation introduced by RR for each wavelength. These were computed in a calibration operation described elsewhere [15, 16].

From S_{OUT}, the degree of polarization (DOP) at each pixel of the image can be calculated as [17]:

$$DOP = \frac{\left(S_1^2 + S_2^2 + S_3^2\right)^{1/2}}{S_0} \qquad (0 \leq DOP \leq 1) \tag{3}$$

Moreover, depolarization can be computed as 1-DOP, which ranges from 0 (totally polarized light) to 1 (depolarized light).

3. Results

3.1. Transmittance

When illuminating the PDCL cell with a collimated laser beam two regions in the transmitted light can be distinguished: central and peripheral (for small and large scattering angles Θ). The central part corresponds to the directional and non-scattered component of the transmitted light and the surrounded areas are associated with the scattered (or diffuse) component of the light. The behaviour of these areas could be very different when changing the voltage and/or the wavelength of the light used for illumination. As a qualitative example, Fig. 2 shows images of the light transmitted through the PDLC cell for the three wavelengths used in this work and three different voltages. As explained above, when using the CCD camera, this imaged the intensity pattern reaching the SC. For this particular case the AU was removed from the system.

For all three wavelengths the behavior of the PDLC in terms of scattering changes as a function of voltage. However the effects caused by the voltage change are more noticeable between 15 and 8 volts. The reduction in voltage is associated with a reduction of the directional component (see below for more details). On the opposite, the scattered component increases with voltage reduction. This is expected since PDLC becomes less transparent with decreasing voltage. For a better understanding of this fact, we also provide some quantitative information in the next two figures.

Figure 3 shows the averaged radial profile of intensity of the light passing the PDLC cell for blue light and two different voltages (30 and 8 volts). Curves were normalized to their maximum values at angle $\Theta = 0$ for a better comparison. As expected the scattering indicatrice becames wider for higher scattering levels, that is, the light intensity levels in peripheral areas are higher for a low voltage.

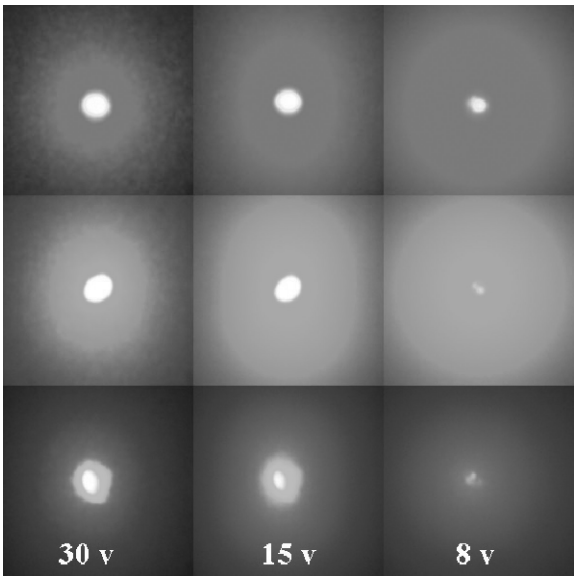

Figure 2. Images of the distribution of light transmitted through the PDLC cell for 30, 15 and 8 volts and three wavelengths. Upper, medium and bottom panels correspond to red, green and blue light beams, respectively. Each image subtends $\sim$ 48 degrees.

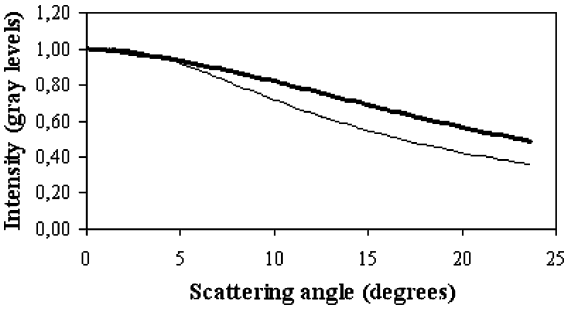

Figure 3. Normalized averaged radial transmittance profile of the scattered light through the PDLC cell for 30 (thin line) and 8 (thick line) volts. Data correspond to blue light.

In order to compare the PDLC scattering effects for the three wavelengths, we also measured the amount of light located in a ring far from the central part of the image (between 16 and 19 degrees) as a function of voltage. Results are depicted in Fig. 4. Overall, for all three wavelengths the intensity of the light located far from the center reduces when voltage increases. The increase in peripheral light between 8 and 30 volts was 51% for red light and 45% for both green and blue.

Figure 5 refers to the behavior of the directional component of the light passing the PDLC cell. It presents the normalized transmittance (in a logarithmic scale) of this directional light for different voltages and wavelengths. As CCD camera had a restricted dynamic range, for these measurements we used the alternative registration setup (inset in Fig. 1).

Results clearly reveal the PDLC transmittance dependence on both voltage and wavelength. For voltages higher than ∼20 volts the transmittance keeps almost constant for all three wavelenghts. However when reducing the voltage, this transmittance rapidly reduces. This effect is more noticeable for lower wavelengths (blue light in our case).

3.2. Spatially Resolved Polarimetry

As a qualitative example Fig. 6 presents the images of the transmitted intensity by the PDLC cell (including both directional and scattered components) for blue light at different

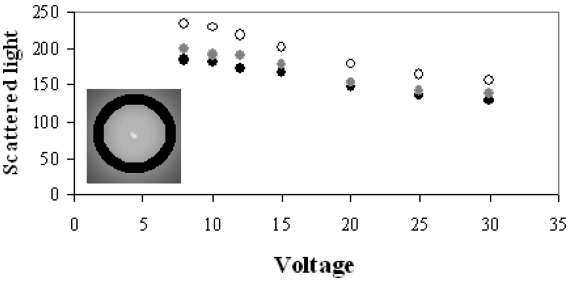

Figure 4. Scattered light in a ring around the center of the image (between 16 and 19 degrees off center) as a function of voltage for red (white symbols), green (grey symbols) and blue (black symbols). Plotted values correspond to the averaged intensity in the ring. The inset indicates the area where the intensity was calculated.

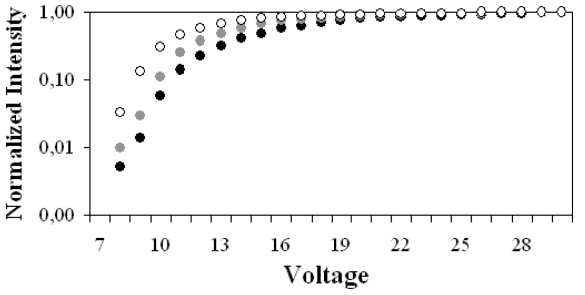

Figure 5. Transmittance of the PDLC cell for the directional component of the light as a funtion of voltage for blue (black circles), green (grey circles) and red (white circles).

values of the azimuth between P1 and P2. These images were registered using the upper configuration in Fig. 1, but excluding RR. As expected, for high scattering level the PDLC cell does not affect much the orientation of the incoming polarization. On the opposite, for low scattering level the maximum found for a parallel configuration tends to disappear.

We finally performed additional polarimetric measurements to calculate the depolarization properties of the PDLC. For this part of the experiment we used the complete analyzer AU (RR plus P2) in Fig. 1. We started by calibrating the complete setup to test the reliability of the instrument. When no sample was included in the polarimeter, the Stokes vector calculated using equation (1) must be that corresponding to the light emerging from P1, that is linear horizontal polarized light (for this operation the alternative registration setup was used). Table 1 shows the reconstructed Stokes vectors obtained for the three wavelenghts. These experimental results are in good agreement with the ideal vector. In view of this, the setup itself does not depolarize the light, which means that all the effects of depolarization would be associated with the PDLC cell.

Series of four polarimetric images (each corresponding to an independent polarization state produced in AU) were registered for different voltages and wavelengths. For these images the complete imaging polarimeter was used (i.e. RR+P2+SC+OB+CCD). Figure 7 presents these images for blue light and three voltages as an example. When a high level of scattering is induced (8 volts, bottom panels), images for the different orientations of the AU look similar. In absence of scattering (30 volts, upper panels) polarimetric images

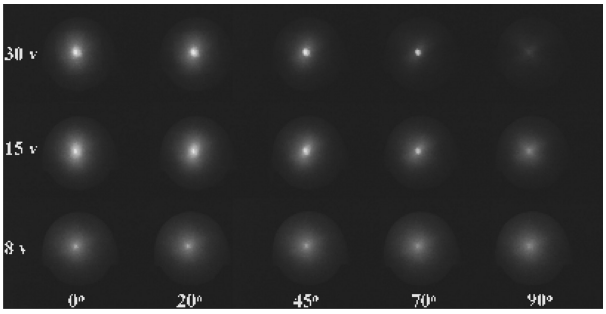

Figure 6. Images of the light scattered by PDLC cell for blue light and three different voltages as a function of the angle between the P1 and P2.

Table 1
Experimental Stokes vectors elements for three different wavelengths when no sample was included in the polarimeter

	Ideal	Blue	Green	Red
S_0	1	1.00	1.00	1.00
S_1	1	0.99	1.00	0.99
S_2	0	0.09	0.09	0.01
S_3	0	−0.01	0.01	0.12

clearly differ. An intermediate case is also shown (15 volts). The central black spot was used to block the directional light and to avoid saturation in the central part of the image. Despite this, the central area of some images was still saturated. Since this could lead to erroneous interpretations of the results, the values corresponding to these areas were excluded from numerical results and deleted from the plots.

Figure 8 presents the corresponding maps for the DOP. Although values are low for the three voltages, some differences can be observed among the maps. For a better understanding, a further analysis of this parameter is given in the following figures. Figure 9 depicts for blue light and three voltages the averaged radial DOP profiles without the central part (as explained above).

Finally Fig. 10 shows the average DOP values for all three wavelengths and five different voltages along the radial profile. Data from the central area data were also excluded. Average DOP values for all wavelengths were 0.03, 0.04, 0.08, 0.15 and 0.21 for 8, 10, 15, 20 and 30 volts respectively.

4. Discussion

We have developed a multispectral polarimeter in transmission mode to study the effects of scattering and depolarization of a PDLC cell. With a configuration polarizer-sample-rotating retarder-polarizer, the system is able to record four independent polarimetric images in order

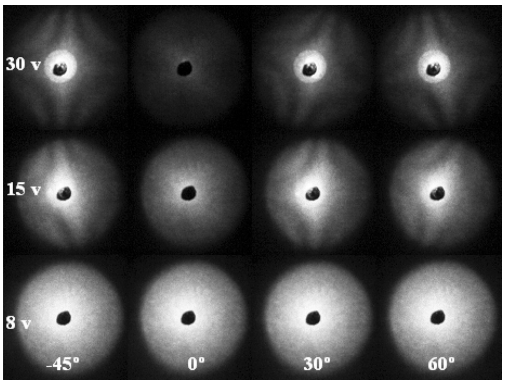

Figure 7. Polarimetric images of the light transmitted through the PDLC cell for blue light and three voltage values. Images subtend the same as in Fig. 2.

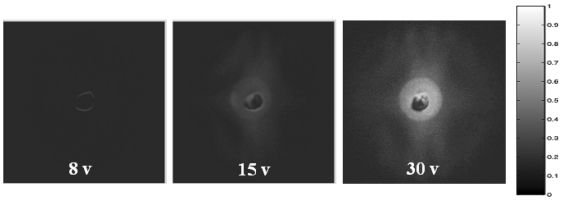

Figure 8. Maps for the DOP for blue light scattered by the PDLC cell at three different voltages. Results were obtained from images in Fig. 8.

to reconstruct the Stokes vector of the light emerging from the sample under study. From this vector the DOP was computed for different amounts of scattering and three wavelengths. The apparatus is flexible enough to be modified according to the requirements of different experimental mesurements.

The PDLC behavior depends on the applied voltage. We used the range between 8 and 30 volts. A subjective observation shows that the lower the voltage, the higher the amount of scatter induced (or alternatively the more milky the appearance). Results have shown that when a light beam passes the PDLC cell, a directional and a scattered component can be distinguished. Transmittance measurements revealed that the former is hardly affected by voltages higher than 20 volts (Fig. 5). However, this rapidly decreases for voltages below 20 volts. The effect is stronger for low wavelengths (blue in our case). The effect of the scattered component also changes with voltage but the behaviour is different from the directional one. When decresing the voltage (that is, when increasing the volume of scattered light) the amount of light located far from the center increases (see for instance Fig. 3). This is a slight increase (approximately linear) that occurs for the three wavelengths, but it is more pronounced for red light. The scattering effects at low voltages are more important for green and blue lights (Fig. 4).

Recently Ozolinsh and Papelba have used PDLC cells to study the impact of induced cataract on visual acuity [14]. The present work compliments results by these authors by including information on both scattering and depolarization.

Nowadays the propagation of light in turbulent media (mainly biological tissues) as well as the study of the effects of scatter on imaging techniques are topics of interest [1–3, 18–21]. Since scattering reduces the contrast of the images in fields such as Astronomy,

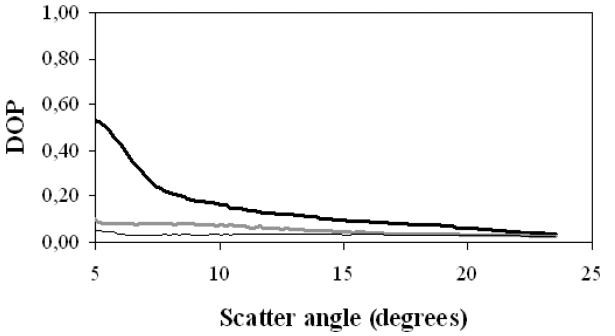

Figure 9. Average DOP radial profile of the scattered light for blue at three different voltages applied to the PDLC cell: 30 (thick black line), 15 (grey line) and 8 (thin black line) volts.

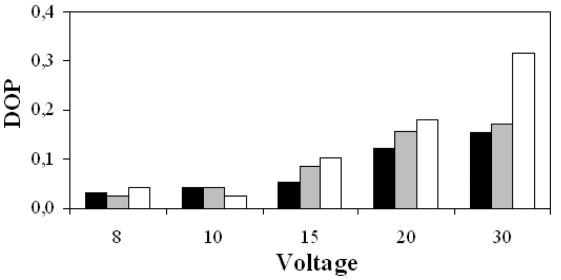

Figure 10. Average DOP of the scattered light along the radial porfile as a function of the voltage for blue (black bars) green (grey bars) and red (white bars). Data corresponding to the central area were not included in the calculation.

Biology or Visual Optics, its quatification would be of interest in order to improve the visibility of objects seen through media containing different levels of scattering. The optical depth-resolved analysis of biological tissues by using OCT imaging is also emerging as an important non-invasive imaging modality [22, 23].

Related to depolarization, our experiments show that the scattered component generated by the PDLC presents low values of DOP, or alternatively, high levels of depolarization. For the best conditions of transparency (30 volts) the mean DOP values were 0.31 for red, 0.17 for green and 0.15 for blue. These values decreased up to 0.04, 0.03 and 0.04, respectively, for the highest scattering condition used here (8 volts). The behavior is similar for all three wavelengths as expected from the measurements of trasmittance of the scattered component.

For the directional component we tested the effect of changing the angle of a polarizer used as an analyzer. For high voltages the intensity of the transmitted light strongly depended on the orientation of this polarizer, with a modulation of more than 0.95. However there is little changes in intensity for large amounts of scatter. This fact is usually associated with depolarized light. Again, this result was found for the three wavelengths used in this experiment.

Polarimetry has previously been used to explore the scattering properties of different media (surfaces, tissues, sphere suspensions, ...) [5–7, 24, 25]. Here we have used it to characterize a scattering-controlled device. The use of a polarimetric parameter such as the DOP as a tool to quantify scattered light [9], has recently been reported. This parameter can be very useful in microscopy and medical imaging among others.

In particular, the living human eye is an optical system were depolarization phenomena occur. Ocular depolarization has been reported to be low in normal eyes [26–28] but it could be important with aging, pathologies or surgical procedures [29–31]. The characterization of PDLC cells in terms of depolarization and the use in visual testing could help in exploring the role of ocular depolarization in visual performance. This could also help in understanding the propagation of depolarized light through the ocular media. Moreover, this may also be important in early diagnosis of ocular pathologies, mainly those related to cataractous proccesses. The analysis of a potential influence of depolarization and scattering on data provided by commercially available setups might also be of great interest.

References

1. J. S. Tyo, M. P. Rowe, E. N. Pugh, Jr., and N. Engheta. Target detection in optically scattering media by polarization-difference imaging, *Appl. Opt.* **35,** 1855–1870 (1996).

2. J. S. Tyo. Enhancement of the point-spread function for imaging in scattering media by use of polarization-difference imaging, *JOSA A* **17**, 1–10 (2000).
3. X. Gan and M. Gu. Image reconstruction through turbid media under a transmission-mode microscope, *J. Biom. Opt*. **7**, 372–377 (2002).
4. S. L. Jacques, R. J. Roman, and K. Lee. Imaging skin pathology with polarized light, *J. Biom. Opt*. **7**, 329–340 (2002).
5. A. H. Hielscher, A. A. Eick, J. R. Mourant, D. Shen, J. P. Freyer, and I. J. Bigio. Diffuse backscattering Mueller matrices of highly scattering media, *Opt. Exp*. **1**, 441–453 (1997).
6. S. Bartel and A. H. Hielscher. Monte Carlo simulations of the diffuse backscattering Muellar matrix for highly scatterng media, *Appl. Opt*. **39**, 1580–1588 (2000).
7. I. Berezhnyy and A. Dogariu. Time-resolved Mueller matrix imaging polarimetry, *Opt. Exp*. **12**, 4635–4649 (2004).
8. D. Pereda Cubián, J. L. Arce Diego, and R. Rentmeesters. Characterization of depolarizing optical media by means of the entropy factor: application to biological tissues, *Appl. Opt*. **44**, 358–365 (2005).
9. J. M. Bueno, E. Berrio, M. Ozolinsh, and P. Artal. Degree of polarization as an objective method of estimating scattering, *JOSA A* **21**, 1316–1321 (2004).
10. F. Jaillon and Saint-Jalmes H. Scattering coefficient determination in turbid media due to backscatterd polarized light, *J. Biom. Opt*. **10**, 034016 (2005).
11. J. K. Ijspeert, P. W. de Waard, T. J. van der Berg, and P. T. de Jong. The intraocular straylight function in 129 healthy volunteers; dependence on angle, age and pigmentation, *Vision Res*. **30**, 699–707 (1990).
12. S. W. Chang, A. Benson, and Azar D. T. Corneal light scattering with stromal reformation after laser in situ keratomileusis. *J. Cataract Refract. Surg*. **24**, 1064–1069 (1998).
13. S. J. Cox, V. Y. Reshetnyak, and T. J. Sluckin. Theory of dielectric and optical properties of PDLC films, *Mol. Crystals Liquid Crystals* **320**, 301–320 (1998).
14. M. Ozolinsh and G. Papelba. Eye cataract simulation using polymer dispersed liquid crystal scattering obstacles, *Ferroelectrics* **304**, 207–212 (2004).
15. J. M. Bueno. Polarimetry using liquid-crystal variable retarders: Theory and calibration *J. Opt. A: Pure Appl. Opt*. **2**, 216–222 (2000).
16. J. M. Bueno. Measurement of parameters of polarization in the living human eye using imaging polarimetry. *Vision Research* **40**, 3791–3799 (2000).
17. R. A. Chipman. "Polarimetry," in *Handbook of Optics*, Vol. 2, 2nd ed., M. Bass, ed. McGraw-Hill, New York. Chap. 22 (1995).
18. B. Pierscionek, R. J. Green, and S. G. Dolgobrodov. Intraocular light scatter as modelled through a stratified medium, *Appl. Opt*. **40**, 6340–6348 (2001).
19. J. Limeres, M. L. Calvo, J. M. Enoch, and V. Lakshminarayanan. Light scattering by an array of birenfringent optical waveguides: Theoretical foundations, *JOSA B* **20**, 1542–1549, (2003).
20. K. Tahir and C. Dainty. Experimental measurements of light scattering form samples with specified optical properties, *J. Opt A: Pure Appl. Opt*. **7**, 207–214 (2005).
21. M. Ozolinsh, I. Lacis, R. Paeglis, A. Sternberg, S. Svanberg, S. Andersson-Engels, and J. Swartling, Electrooptic PLZT ceramics devices for vision scaience applications, *Ferroelectrics* **273**, 131–136 (2002).
22. S. Jiao, G. Yao, and L. Wang. Depth-resolved two-dimensional Stokes vectors of backscattered light and Mueller matrices of biological tissue measured with optical coherence tomography, *Appl. Opt*. **39**, 6318–6324 (2000).
23. J. F. de Boer and T. E. Milner. Review of polarization sensitive optical coherence tomography and stokes vector determination, *J. Biomed. Opt*. **7,** 359–371 (2002).
24. B. Kaplan, E. Compain, and B. Drevillon. Phase-modulated Mueller ellipsometry characterization of scattering by latex suspensions, *Appl. Opt*. **39**, 629–636 (2000).
25. R. Espinosa-Luna. Scattering by rough surfaces in a conical configuration: experimental Mueller matrix, *Opt. Lett*. **27**, 1510–1512 (2002).

26. W. N. Charman. Reflection of plane-polarized light by the retina, *British Journal of Physiological Optics* **34**, 34–49 (1980).
27. G. J. van Blokland and D. van Norren. Intensity and polarization of light scattered at small angles from the human fovea. *Vision Res.* **26**, 485–94 (1986).
28. J. M. Bueno. Depolarization effects in the human eye, *Vision Res.* **41**, 2687–2696 (2001).
29. J. M. Bueno. The influence of depolarization and corneal birefringence on ocular polarization, *Journal of Optics A: Pure and Applied Optics* **6**, S91–S99 (2004).
30. S. A. Burns, A. E. Elsner, M. B. Mellem-Kairala, and R. B. Simmons. Improved contrast of subretinal structures using polarization analysis, *Investigative Ophthalmology and Vision Science* **44**, 4061–4068 (2003).
31. J. M. Bueno, E. Berrio, and P. Artal. Corneal polarimetry after LASK refractive surgery. *J. Biomed. Opt.* **45**, 014001 (2006).